Journal of Biomedical Optics

SPIEDigitalLibrary.org/jbo

Optical coherence tomography based microangiography for quantitative monitoring of structural and vascular changes in a rat model of acute uveitis *in vivo*: a preliminary study

Woo June Choi
Kathryn L. Pepple
Zhongwei Zhi
Ruikang K. Wang

SPIE

Optical coherence tomography based microangiography for quantitative monitoring of structural and vascular changes in a rat model of acute uveitis *in vivo*: a preliminary study

Woo June Choi,[a] Kathryn L. Pepple,[b] Zhongwei Zhi,[a] and Ruikang K. Wang[a,b,*]
[a]University of Washington, Department of Bioengineering, Seattle 98195, Washington, United States
[b]University of Washington, Department of Ophthalmology, Seattle 98104, Washington, United States

Abstract. Uveitis models in rodents are important in the investigation of pathogenesis in human uveitis and the development of appropriate therapeutic strategies for treatment. Quantitative monitoring of ocular inflammation in small animal models provides an objective metric to assess uveitis progression and/or therapeutic effects. We present a new application of optical coherence tomography (OCT) and OCT-based microangiography (OMAG) to a rat model of acute anterior uveitis induced by intravitreal injection of a killed mycobacterial extract. OCT/OMAG is used to provide noninvasive three-dimensional imaging of the anterior segment of the eyes prior to injection (baseline) and two days post-injection (peak inflammation) in rats with and without steroid treatments. OCT imaging identifies characteristic structural and vascular changes in the anterior segment of the inflamed animals when compared to baseline images. Characteristics of inflammation identified include anterior chamber cells, corneal edema, pupillary membranes, and iris vasodilation. In contrast, no significant difference from the control is observed for the steroid-treated eye. These findings are compared with the histology assessment of the same eyes. In addition, quantitative measurements of central corneal thickness and iris vessel diameter are determined. This pilot study demonstrates that OCT-based microangiography promises to be a useful tool for the assessment and management of uveitis *in vivo*.
[DOI: 10.1117/1.JBO.20.1.016015]

Keywords: optical coherence tomography; optical microangiography; acute anterior uveitis; ocular inflammation; experimental rat model.

Paper 140735R received Nov. 6, 2014; accepted for publication Dec. 19, 2014; published online Jan. 16, 2015.

1 Introduction

Optical coherence tomography (OCT) is a well-established optical imaging modality that can provide three-dimensional (3-D) information of tissue scattering in a biological sample.[1] OCT is advantageous because of its noninvasiveness, micrometer resolution, real-time, and depth-resolved imaging, making it a powerful tool in the investigations of subtle morphological or functional changes in biological tissues in a variety of biomedical and clinical applications.[2–4] This technique is also favorable for the serial observation of disease progression[5–7] because of its *in vivo* imaging capability without a need for excision of the specimen or postmortem histology at different time-points. These OCT features are especially important for ophthalmic imaging because the eye is a clear media to light and consists of thin layered structures, allowing easy access of the OCT beam to the intraocular structures, such as retinal layers. OCT has proven clinically successful in the assessment of several intraocular diseases and conditions, such as age-related macular degeneration, diabetic retinopathy, and glaucoma.[8–10]

Uveitis is one of the intraocular conditions describing the inflammation of the uveal tract of the eye, including the iris, ciliary body (CB), and choroid.[11] It represents a major cause of visual impairment, ultimately resulting in vision loss, accounting for 10% of all cases of legal blindness worldwide.[12,13] Over the decades, the experimental rodent models of uveitis have been extensively used as an effective preclinical model to understand the pathogenesis of human uveitis and evaluate the therapeutic efficacy of new medications because of their resemblance in immunopathogenic mechanisms to the human uveitis.[14–17] To observe ocular inflammation in the small animal models, slit-lamp microscopy[18] and fluorescein angiography (FA)[19] have been used as the primary methods where the severity of inflammation is determined by either counting the infiltrating cells in the anterior chamber (AC)[18] or detecting vascular disorders in the posterior segment.[19] However, the use of slip-lamp microscopy to grade cells is quite subjective, depending on the empirical ability of the cell graders. Also, the FA is limited to qualitative angiographic analysis in two-dimensions (2-D). Recent ophthalmic OCT studies have shown one possibility for the quantitative assessment of the posterior uveitis in experimental murine models.[20–23] The results indicate that OCT could become an effective assay tool for the longitudinal monitoring of pathological changes in the retinal lesions during uveitis.[20–23]

In this paper, we report a new application of OCT and OCT-based microangiography (OMAG)[24–28] to a rodent model of anterior uveitis. Acute anterior uveitis (AAU) is the commonest form of uveitis with single episodes of sudden onset and limited

*Address all correspondence to: Ruikang K. Wang, E-mail: wangrk@uw.edu

0091-3286/2015/$25.00 © 2015 SPIE

duration, involving the inflammation of the AC, iris, and CB.[29,30] Although anterior uveitis is a less common cause of blindness than posterior uveitis, it often can lead to severe ocular morbidity after the onset if left untreated. The aim of the study is to assess the efficacy of OCT/OMAG for the quantitative monitoring of structural and functional changes in the anterior segment during AAU in the rat model.

2 Materials and Methods

2.1 *Animal Preparation*

Two female Lewis rats weighing 125 to 149 g were purchased from Harlan Laboratories and maintained with standard chow and water *ad libitum* under pathogen-free conditions. All animals were treated in accordance with the ARVO statement for the Use of Animals in Ophthalmic and Vision Research under the animal protocol approved by the Animal Care and Use Committee of University of Washington.

2.2 *OCT-Based Microangiography*

An anterior OCT system was used to implement OMAG, which was the system previously described in Ref. 31. In brief, it was a custom-built spectral-domain OCT system operated at a central wavelength of 1340 nm with a scan speed of 92,000 A lines per second. The spatial (axial × lateral) resolution of the system was 7 μm × 7 μm in air, respectively. The system sensitivity was measured at 100 dB at the focal spot of the sample beam, corresponding to 0.5 mm below the zero delay line.

The rat was anesthetized with inhalational isoflurane (1.5%) mixed with 20% oxygen. Each animal was placed in the right lateral decubitus position and secured in a custom-made stereotactic stage equipped with a heating pad and a nose cone for continuous inhaled isoflurane anesthesia. Complete exposure of the anterior segment was provided by traction sutures placed through the lower and upper eyelids, and cornea protection was provided with a topical balanced salt solution (BSS, Alcon, Johns Creek, GA) throughout the imaging session. The stereotactic stage was then positioned with the apex of the cornea centered beneath a scan lens in the sample arm of the OCT system.

A repetitive B-mode step scanning protocol[32] was adopted to implement OMAG, in which five repeated B-scans (fast scan) at each C-scan (slow scan) position were performed on the anterior segment of the rat eye at a speed of 140 frames per second. This scanning protocol generated a total of 2000 B-frames (512 A lines per each B-frame) in a single 3-D OCT data volume. During the image acquisition, anesthesia was maintained using a breathing anesthesia machine (M3000, Supera Anesthesia Innovations, Clackamas, OR) to restrain bulk motions from its body except for breathing and pulsation.

B-mode blood flow images were computed from the acquired 3-D OCT data volume by applying an intensity-based OCT angiography algorithm.[31] In this method, the intensity changes in time caused by randomly backscattered lights resulting from moving red blood cells in the vessel lumens can be decoupled from the surrounding static tissue regions by subtraction of adjacent two B-frames (a time interval of 7 ms) obtained at the same location, representing blood perfusion in the functional vessels. This strategy to contrast blood flow is quite similar to ultrahigh-sensitive optical microangiography,[25,26] an OMAG algorithm that utilizes the analytical forms of the OCT signals rather than the OCT amplitude signals. Using five repetition B-scans, one blood flow image was obtained through ensemble averaging of the calculated four B-scans of blood flow at a given C-scan position. Eventually, a total of 400 cross-sectional blood flow images together with the corresponding 400 structural images were reconstructed within the scanned tissue volume. To facilitate the visualization and analyses, the 3-D blood flow data were collapsed into an *en face* (XY) projection image (an OCT angiogram).

2.3 *Induction of Acute Anterior Uveitis*

The experimental protocol for the rat model of AAU is illustrated in Fig. 1. To induce AAU, we modified an established experimental model of uveitis previously reported in rabbits to the rat.[33] Anterior uveitis was initiated in the right eye of each rat with an intravitreal injection of 10 μg of killed mycobacterium tuberculosis H37Ra antigen (DifcoLaboratories, Detroit, MI) in a 5 μl volume of phosphate buffered saline at day 0. This protocol induces intraocular inflammation that peaks at two days post-injection. To test the therapeutic effect of steroid treatment on AAU, the other rat was also treated with an additional periocular injection of steroids, 4 mg triamcinolone in 0.1 ml at day 0. The steroid is a potent anti-inflammatory agent. Anterior OCT imaging was performed with the right eyes of all rats at day 0 (preinjection) and at day 2 (peak-inflamed or steroid treated).

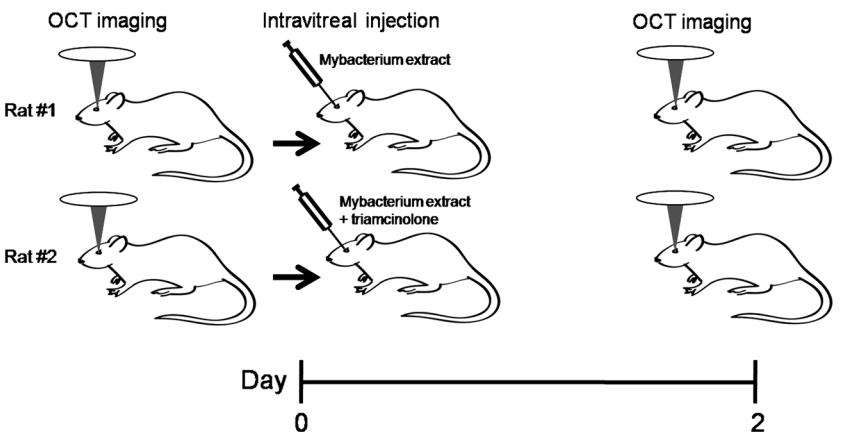

Fig. 1 Illustration of the experimental protocol for the rat model of acute anterior uveitis.

2.4 *Histology*

After OCT imaging at day 2, the animals were euthanized and eyes were collected for histology. The collected eyes were fixed in 10% neutral buffered formalin (Triangle Biosciences, Durham, NC) and embedded in paraffin. 4-μm sections were obtained and stained with hematoxylin and eosin for microscopic evaluation.

3 Results

3.1 *Identification of Inflammation in the Rat Anterior Segment*

The signs of intraocular inflammation *in vivo* include the infiltration of white blood cells (WBCs) into the AC and posterior chamber (PC), corneal edema, iris vascular dilation, and an increase in the protein concentration in the intraocular fluids.[18,34] When inflammation is severe, the protein concentration can form an inflammatory membrane on the anterior surface of the iris and across the pupil.[18] To determine if OCT imaging could identify these features in a rodent model of anterior uveitis, we obtained OCT images at baseline and during peak inflammation and compared these to histology. Figure 2 shows the representative cross-sectional OCT images obtained at the central AC [Figs. 2(a) and 2(c)] and at the limbus [Figs. 2(b) and 2(d)]. At day 0, the OCT images [Figs. 2(a) and 2(b)] reveal typical anatomical features of the anterior segment of normal murine, including the hyper-reflective cornea, iris and CB, the optically empty AC, and the lens.[35] At day 2, the OCT images [Figs. 2(c) and 2(d)] reveal the inflammatory cell infiltration into both the anterior and posterior chambers and along the anterior lens capsule [arrows in Figs. 2(c) and 2(d)], the increase of corneal thickness [oblique bars in Figs. 2(a) and 2(c)], and fibrinous membranes on the surface of the iris and extending across the pupil [asterisks in Fig. 2(c)]. An unexpected finding was the increase in OCT signal intensity of the zonules during inflammation [dotted circle in Fig. 2(d)]. The zonules are a series of fibrous strands connecting the CB with the lens. At day 0, they can be seen as individual thin hyper-reflective bands, but at day 2, the individual fibers are obscured probably because of the surrounding inflammatory cells. Post mortem histology [Fig. 2(e)] confirms the inflammatory changes noted by the OCT images. An additional note regarding the OCT imaging is that the sclera in Fig. 2(d) looks down-curved, which is caused by the refractive index difference between the hydration medium (BSS) on the sclera and the air.

3.2 *Identification of Steroid Treatment Effect on Inflammation of the Rat Anterior Segment*

Histology is the gold standard for the detection of intraocular inflammation in animal models of uveitis. To compare the ability of OCT with histology in the assessment of the effect of steroid treatment on inflammation, the rat induced with AAU was treated with the periocular injection of triamcinolone. OCT images of the eye were obtained at day 0 and day 2 as shown in Fig. 3. In contrast to the rat without treatment (see Sec. 3.1), at day 2, no inflammatory changes are detected by OCT images [Figs. 3(c) and 3(d)] when compared to the baseline [Figs. 3(a) and 3(b)] in the steroid-treated animal. This finding is confirmed with the histologic assessments [Fig. 3(e)] by the absence of infiltrating WBCs in the AC, PC, or surrounding the CB and the zonules. These data are consistent with clinical results in

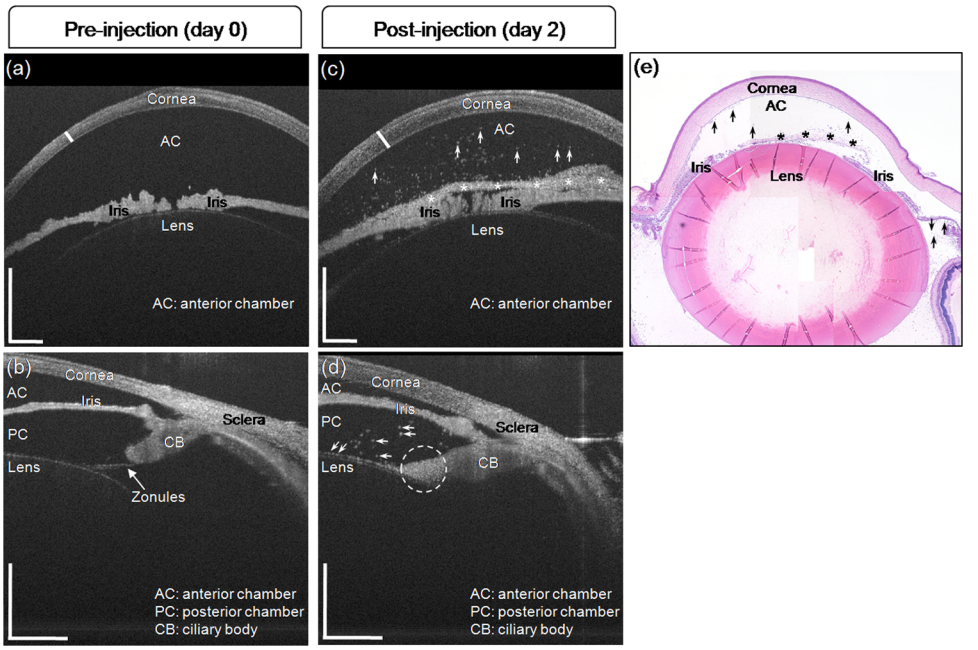

Fig. 2 *In vivo* optical coherence tomography (OCT) imaging of the anterior segment in the rat model of acute anterior uveitis. (a) and (b) Representative cross-sectional OCT structural images obtained at central anterior chamber (AC) and at limbal region at day 0 (baseline), respectively. (c) and (d) Representative cross-sectional OCT structural images obtained at the location similar to (a) and (b) at day 2 (peak inflammation), respectively, showing structural changes, such as infiltrating cells (arrows) in the AC and the posterior chamber (PC), thickened cornea, and fibrinous membranes (asterisks) on the surface of iris and across the pupil. The inflammation features in the OCT images [(c) and (d)] are confirmed with a histologic section through the anterior segment of the same rat eye (e). Sale bars: 500 μm.

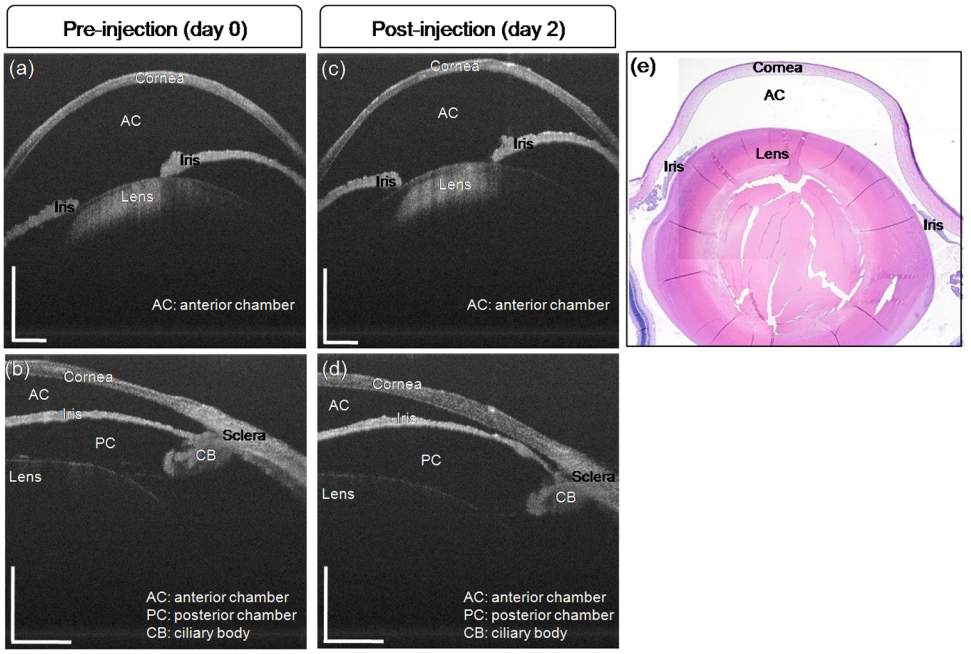

Fig. 3 *In vivo* OCT imaging before and after steroid treatment in the acute anterior uveitis rat model. (a) and (b) Representative cross-sectional OCT structural images obtained at AC and at the limbal region at day 0 (baseline), respectively. (c) and (d) Representative cross-sectional OCT structural images obtained at the location similar to (a) and (b) at day 2 (steroid treatment), respectively, showing no significant change in morphology compared to the baseline [(a) and (b)]. The anti-inflammation features in the OCT images [(c) and (d)] are confirmed with a histologic section through the anterior segment of the same rat eye (e). Scale bars: 500 μm.

humans that triamcinolone effectively inhibits ocular inflammatory activity in patients with uveitis.[36]

3.3 *Quantification of Central Corneal Thickness Changes*

To quantify the central corneal thickness (CCT) changes in rats with and without steroid treatment, the central cornea was defined to the area [2.6 mm (X) × 2.6 mm (Y)] centered on the pupil. The thickness across this area was determined using a semiautomatic segmentation algorithm.[37] A resulting 2-D CCT map was obtained from the segmented 3-D corneal information. Figure 4 shows the average corneal thickness obtained at day 0 and day 2 for the inflamed and steroid-treated animals, respectively. For the rat without steroid treatment [Fig. 4(a)], the CCT at day 2 (166.79 ± 12.45 μm) is more than 1.3 times thicker than the CCT at day 0 (121.29 ± 8.16 μm). This is consistent with clinical findings of corneal edema in human patients with uveitis.[34] For the rat treated with the steroid, the CCT at day 2 (74.81 ± 8.23 μm) was not increased when compared with day 0 (76.32 ± 5.06 μm). This is consistent with the absence of inflammation in the presence of steroids as assessed by histology.

3.4 *Quantification of Iris Vascular Changes Using OCT Angiograms*

We also investigated blood perfusion changes in the rat iris during acute inflammation using OMAG. This angiographic modality was able to delineate functional microvasculature in the anterior segment tissue beds of the rat eyes *in vivo*.[31] Figure 5 shows microvascular imaging results for the rat without steroid treatment. An *en face* (XY) OMAG (3.57 mm × 3.57 mm)

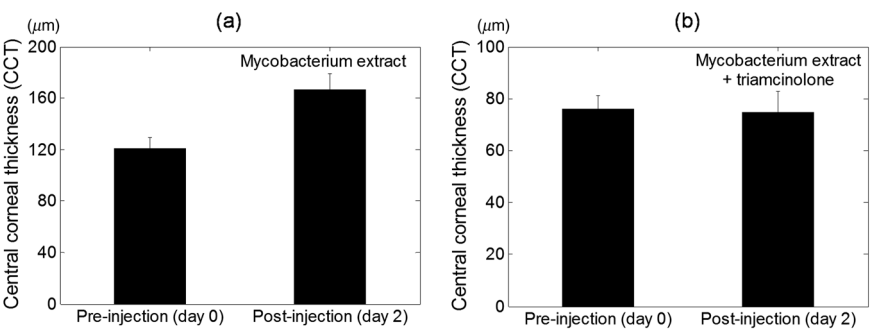

Fig. 4 Changes in central corneal thickness of the peak inflamed rat (a) without and (b) with the steroid treatment.

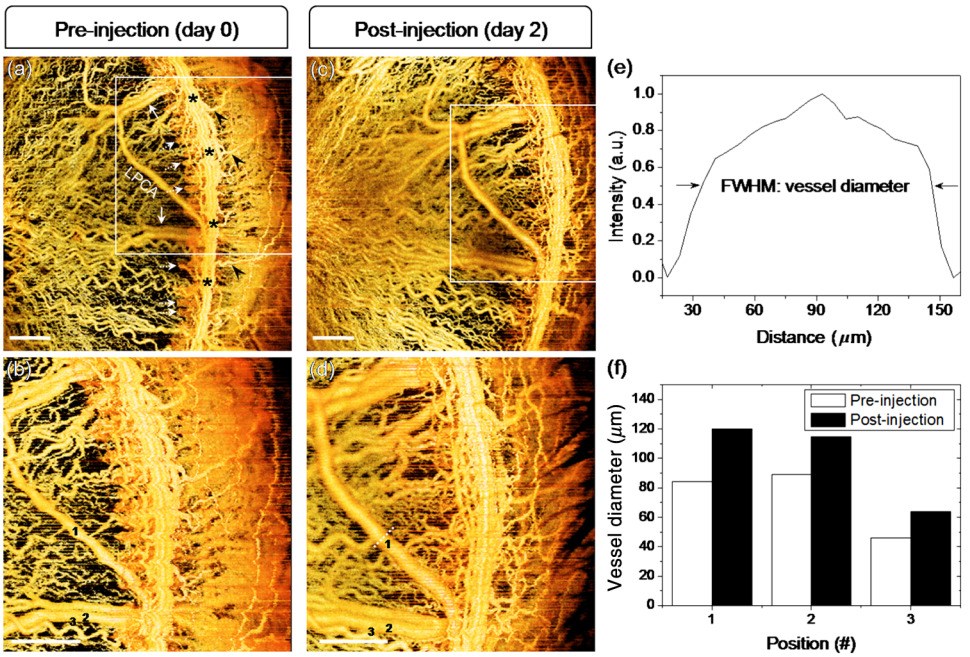

Fig. 5 *In vivo* OCT-based microangiography (OMAG) imaging of anterior segment vasculature in the anterior uveitis rat model. (a) and (c) Two-dimensional (2-D) *en face* (XY) OMAG angiograms [3.57 mm (X) × 3.57 mm (Y)] of the anterior segment of the rat eye at day 0 (baseline) and day 2 (peak inflammation), respectively. Compared to (a), in (c), the dilation of the iris vessels, including a long posterior ciliary artery (LPCA) and radial iris vessels [solid arrows in (a)], is evident and the presence of the ciliary plexus [dotted arrows in (a)] is obscured. These results are better appreciated with higher magnification angiographic views (b) and (d) from the smaller scanned area [2.1 mm (X) × 2.1 mm (Y)], indicated as white boxes in (a) and (c), respectively. (e) A normalized intensity line profile across the location 1 on the LPCA [dotted line in (d)]. Its FWHM represents the vessel diameter. In (f), the iris vascular dynamics is quantified with the vessel diameters measured at three locations (1, 2, and 3) on the iris vessels in (b) and (d). Scale bars: 500 μm.

of the anterior segment in the rat eye at day 0 (baseline) [Fig. 5(a)] illustrates the complex microvascular anatomy of the anterior segment, consisting of radial iris vessels (solid arrows), long posterior ciliary arteries (LPCA), circumferential ciliary plexus (dotted arrows) in the ciliary process located behind the iris, and limbal plexus (asterisks) supplied by aqueous-containing veins (arrow heads). The OMAG angiogram at day 2 [Fig. 5(c)] shows that the iris vessels become dilated, and the ciliary plexus is obscured when compared to the day 0 images. However, the limbal circulation is almost not affected. Higher-magnification OMAG angiograms of the region from smaller scanned areas (2.1 mm × 2.1 mm) highlight these differences [Figs. 5(b) and 5(d)].

To quantify the amount of vascular dilation that occurs with inflammation, we compared iris vessel diameters at the same location for the pre and postinjection OMAG angiograms. Three iris vessels were chosen and marked with numbers in Figs. 5(b) and 5(d), and the vessel diameters at the numbered

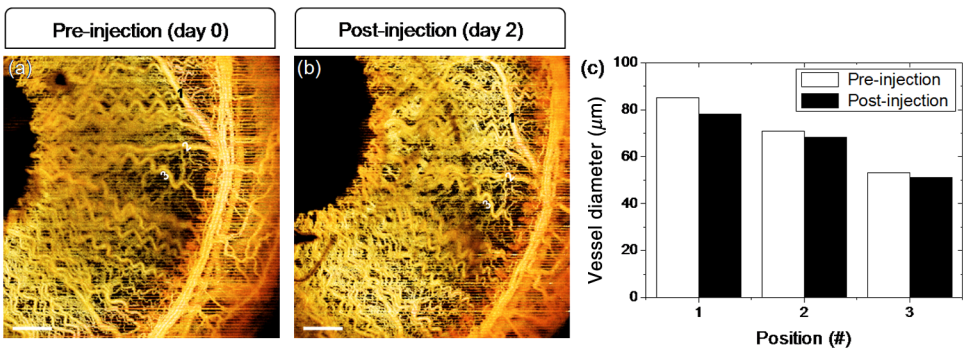

Fig. 6 *In vivo* OMAG imaging of the anterior segment with the addition of steroid treatment to the acute anterior uveitis rat model. (a) and (b) 2-D *en face* (XY) OMAG angiograms [3.57 mm (X) × 3.57 mm (Y)] of the anterior segment in the rat eye at day 0 (baseline) and at day 2 (steroid treatment), respectively. Compared to the baseline (a), no appreciable changes in vasculature are observed for the steroid treated eye (b). (c) Comparison of iris vessel diameters at three locations (1, 2, and 3) on the iris vessels in (a) and (b). Scale bars: 500 μm.

locations were calculated as a full width at half maximum (FWHM) of the normalized intensity line profile across each vessel.[38] Figure 5(e) shows a typical normalized intensity line profile across location 1 (dotted line) on the LPCA in Fig. 5(d). At this point, the FWHM of the LPCA was measured as 119.8 μm, corresponding to the vessel diameter at day 2. The iris vessel diameters of three vessels were compared at day 0 and day 2 [Fig. 5(f)]. On average, the vessel diameters at day 2 are 30 to 40% greater than those at day 0. This is consistent with clinical findings of the iris vessel dilation in human patients with AAU.[39]

To determine if the iris vascular changes could be detected in the presence of steroid treatment, the anterior microcirculation of the treated rat was visualized with OMAG angiograms (3.57 mm × 3.57 mm) as shown in Fig. 6. In the steroid-treated eye, the vasculature [Fig. 6(b)] exhibits no appreciable difference when compared to the baseline images [Fig. 6(a)], including the qualitative appearance of the iris and limbal vascular caliber and the visibility of the CB. Iris vessel diameters were then quantified using the three numbered iris vessels in Figs. 6(a) and 6(b), and plotted in Fig. 6(c). There was no obvious increase in vessel diameter. Interestingly, we did identify a small but not significant decrease in the vessel diameter of ~10% in the steroid-treated eye. It is well known that the steroid we used (triamcinolone) has specifically profound antiangiogenic, antipermeability, and vasoconstrictive effects in addition to relieving inflammatory responses.[40] Therefore, we expect that the overall decrease in iris vessel diameters may be primarily due to such vascular effects due to the steroid applied to the inflamed rat eye.

4 Discussion and Summary

In this study, we have developed a novel OCT protocol including OCT-based microangiography and applied it to an acute anterior uveitis model in rats. The OCT findings revealed typical pathological and vascular changes associated with inflammation. These findings include corneal swelling, cellular infiltration in the anterior and posterior chambers, fibrinous membranes on the pupil, and dilation in the iris vessels. We also showed that the effect of steroid treatment on inflammation can be detected by OCT. Importantly, these imaging findings were supported by histologic assessments conducted on the same animals.

One of the strengths of the imaging assays in uveitis is the ability to use the imaging data to objectively quantify the level of inflammation. We have shown here that corneal thickness and iris vascular diameter can be quantified from the anterior segment OCT datasets obtained in rats. Although we had a limited dataset, this pilot study suggests that the corneal thickness and vascular caliber are good candidates for quantification since they increase in the presence of inflammation, but not when treated by steroids. In addition, although not addressed in this study, OCT imaging is capable of providing the quantitative measures for the infiltrating cells in both the anterior and posterior chambers, and zonule inflammation as shown in Fig. 2.

The murine models of uveitis have similarities to the spectrum of immunopathogenic features of human uveitis and have served as preclinical models to study the fundamental mechanism of the uveitic disease and to test for the response to new therapeutic strategies. An *in vivo* longitudinal study of the same individual is, thus, essential in the monitoring of pathological and functional changes during uveitis for the quantification of the extent of the disease progression.

We identified a few challenges that will need to be addressed in future OCT studies of the anterior segment. First, the custom-made system does not have sequential image registration capacity, which led to a difficulty in precisely locating the same region of interest for day 0 and day 2 images. Second, for anterior OCT imaging, ocular tissue refraction of the OCT beam can distort the physical geometry of the anterior segment in an OCT image. The refraction effect was not considered in this initial study, which would make the measurements somehow different from their actual dimensions. The reliability of these quantitative parameters can be reinforced with correction of the optical distortion considering the refractive indices of ocular tissue layers.[41] Third, the iris vasculature caliber and tortuosity could be affected by pupillary dilation. Although we used the same lighting conditions (ambient illumination) for all studies, we noted the variation in pupil size. The pupil size needs to be constant through all imaging sessions to minimize the effect due to environmental factors that may affect iris vasculature calibers, so that the quantitative measurements of iris vessel diameter in inflammation and treatment can be reproducible. Addressing these challenges will result in improving this technique for future large-scale and long-term studies.

In summary, this study demonstrates the feasibility of OCT/OMAG in the quantitative assessment of anterior segment inflammation in an experimental murine model of uveitis. Longitudinal imaging and automated quantification of the structural and vascular changes in the anterior segment of the uveitic eyes will be a useful tool in the investigations of the mechanisms of ocular inflammation and in the preclinical testing of new therapeutic treatment strategies for uveitis. Future studies will include the application of these techniques to the diagnosis and management of anterior uveitis in humans.

Acknowledgments

This work was supported in part by a Latham Vision Research Innovation Award, a Research to Prevent Blindness Innovation Award, and a research grant from the National Eye Institute (R01 EY024158). Dr. Pepple is also supported by a research grant from the National Eye Institute (K08 EY0123998). The content is solely the responsibility of the authors and does not necessarily represent the official views of the grant-giving bodies.

References

1. J. G. Fujimoto et al., "Optical coherence tomography: an emerging technology for biomedical imaging and optical biopsy," *Neoplasia* **2**(1–2), 9–25 (2000).
2. B. E. Bouma et al., "Fourier-domain optical coherence tomography: recent advances toward clinical utility," *Curr. Opin. Biotechnol.* **20**(1), 111–118 (2009).
3. F. T. Nguyen et al., "Intraoperative evaluation of breast tumor margins with optical coherence tomography," *Cancer Res.* **69**(22), 8790–8796 (2009).
4. A. M. Zysk et al., "Optical coherence tomography: a review of clinical development from bench to bedside," *J. Biomed. Opt.* **12**(5), 051403 (2007).
5. R. K. Chhetri et al., "Longitudinal study of mammary epithelial and fibroblast co-cultures using optical coherence tomography reveals morphological hallmarks of pre-malignancy," *PLoS One* **7**(11), e49148 (2012).
6. R. Silver et al., "Using optical coherence tomography for the longitudinal noninvasive evaluation of epidermal thickness in a murine model of chronic skin inflammation," *Skin Res. Technol.* **18**(2), 225–231 (2012).

7. K. M. Poole et al., "Longitudinal study of arteriogenesis with swept source optical coherence tomography and hyperspectral imaging," *Proc. SPIE* **8934**, 89341Z (2014).
8. P. A. Keane et al., "Evaluation of age-related macular degeneration with optical coherence tomography," *Surv. Ophthalmol.* **57**(5), 389–414 (2012).
9. J. C. Buabbud, M. M. Al-latayfeh, and J. K. Sun, "Optical coherence tomography imaging for diabetic retinopathy and macular edema," *Curr. Diab. Rep.* **10**(4), 264–269 (2010).
10. J. M. Wessel et al., "Longitudinal analysis of progression in glaucoma using spectral-domain optical coherence tomography," *Invest. Ophthalmol. Vis. Sci.* **54**(5), 3613–3620 (2013).
11. C. M. Guly and J. V. Forrester, "Investigation and management of uveitis," *BMJ* **341**, 821–826 (2010).
12. M. S. A. Suttorp-Schulten and A. Rothova, "The possible impact of uveitis in blindness: a literature survey," *Br. J. Ophthalmol.* **80**(9), 844–848 (1996).
13. N. R. Acharya et al., "Incidence and prevalence of uveitis: results from the Pacific Ocular Inflammation Study," *JAMA Ophthalmol.* **131**(11), 1405–1412 (2013).
14. J. T. Rosenbaum et al., "Endotoxin-induced uveitis in rats as a model for human disease," *Nature* **286**(5773), 611–613 (1980).
15. R. Hoekzema et al., "Endotoxin-induced uveitis in the rat: the significance of intraocular interleukin-6," *Invest. Ophthalmol. Vis. Sci.* **33**(3), 532–539 (1992).
16. G. Pennesi et al., "A humanized model of experimental autoimmune uveitis in HLA class II transgenic mice," *J. Clin. Invest.* **111**(8), 1171–1180 (2003).
17. U. C. S. Yadav, S. Subramanyam, and K. V. Ramana, "Prevention of endotoxin-induced uveitis in rats by benfotiamine, a lipophilic analogue of vitamin B1," *Invest. Ophthalmol. Vis. Sci.* **50**(5), 2276–2282 (2009).
18. R. V. Agrawal et al., "Current approach in diagnosis and management of anterior uveitis," *Indian J. Ophthalmol.* **58**(1), 11–19 (2010).
19. C. P. Herbort, "Fluorescein and indocyanine green angiography for uveitis," *Middle East Afr. J. Ophthalmol.* **16**(4), 168–187 (2009).
20. I. Gadjanski et al., "Correlation of optical coherence tomography with clinical and histopathological findings in experimental autoimmune uveoretinitis," *Exp. Eye Res.* **93**(1), 82–90 (2011).
21. K. Harimoto et al., "Evaluation of mouse experimental autoimmune uveoretinitis by spectral domain optical coherence tomography," *Br. J. Ophthalmol.* **98**(6), 808–812 (2014).
22. J. Chen et al., "Use of optical coherence tomography and electroretinography to evaluate retinal pathology in a mouse model of autoimmune uveitis," *PLoS One* **8**(5), e63904 (2013).
23. C. J. Chu et al., "Assessment and *in vivo* scoring of murine experimental autoimmune uveoretinitis using optical coherence tomography," *PLoS One* **8**(5), e63002 (2013).
24. R. K. Wang and L. An, "Doppler optical micro-angiography for volumetric imaging of vascular perfusion *in vivo*," *Opt. Express* **17**(11), 8926–8940 (2009).
25. L. An, J. Qin, and R. K. Wang, "Ultrahigh sensitive optical microangiography for *in vivo* imaging of microcirculations within human skin tissue beds," *Opt. Express* **18**(8), 8220–8228 (2010).
26. L. An, T. T. Shen, and R. K. Wang, "Using ultrahigh sensitive optical microangiography to achieve comprehensive depth resolved microvasculature mapping for human retina," *J. Biomed. Opt.* **16**(10), 106013 (2011).
27. J. Enfield, E. Jonathan, and M. Leahy," *In vivo* imaging of the microcirculation of the volar forearm using correlation mapping optical coherence tomography (cmOCT)," *Opt. Express* **2**(5), 1184–1193 (2011).
28. A. Mariampillai et al., "Optimized speckle variance OCT imaging of microvasculature," *Opt. Lett.* **35**(8), 1257–1259 (2010).
29. D. J. Careless and R. D. Inman, "Acute anterior uveitis: clinical and experimental aspects," *Semin. Arthritis Rheum.* **24**(6), 432–441 (1995).
30. A. D. Birnbaum et al., "Bilateral simultaneous-onset nongranulomatous acute anterior uveitis," *Arch. Ophthalmol.* **130**(11), 1389–1394 (2012).
31. W. J. Choi, Z. Zhi, and R. K. Wang, "*In vivo* OCT microangiography of rodent iris," *Opt. Lett.* **39**(8), 2455–2458 (2014).
32. R. K. Wang et al., "Depth-resolved imaging of capillary networks in retina and choroid using ultrahigh sensitive optical microangiography," *Opt. Lett.* **35**(9), 1467–1469 (2010).
33. C.-K. Cheng et al., "Intravitreal sustained-release dexamethasone device in the treatment of experimental uveitis," *Invest. Ophthalmol. Vis. Sci.* **36**(2), 442–453 (1995).
34. T. Olsen, "Change in the corneal endothelium after acute anterior uveitis as seen with the specular microscope," *Acta Ophthalmol.* **58**(2), 250–256 (1980).
35. J. J. Liu et al.," *In vivo* imaging of the rodent eye with swept source/Fourier domain OCT," *Biomed. Opt. Express* **4**(2), 351–363 (2013).
36. A. A. Okada et al., "Trans-Tenon's retrobulbar triamcinolone infusion for the treatment of uveitis," *Br. J. Ophthalmol.* **87**(8), 968–971 (2003).
37. X. Yin, J. R. Chao, and R. K. Wang, "User-guided segmentation for volumetric retinal optical coherence tomography images," *J. Biomed. Opt.* **19**(8), 086020 (2014).
38. D. X. Hammer et al., "Longitudinal vascular dynamics following cranial window and electrode implantation measured with speckle variance optical coherence tomography," *Biomed. Opt. Express* **5**(8), 2823–2836 (2014).
39. P. N. Dayani, "Acute anterior uveitis: an overview," 2010, http://eyetubeod.com/2010/10/acute-anterior-uveitis-an-overview (23 December 2014).
40. S. M. Couch and S. J. Bakri, "Intravitreal triamcinolone for intraocular inflammation and associated macular edema," *Clin. Ophthalmol.* **3**, 41–47 (2009).
41. P. Li et al., "In vivo microstructural and microvascular imaging of the human corneo-scleral limbus using optical coherence tomography," *Biomed. Opt. Express* **2**(11), 3109–3118 (2011).

Biographies of the authors are not available.